ADVANCED FUNCTIONAL MATERIALS
www.afm-journal.de

Oxygen Vacancy Creation, Drift, and Aggregation in TiO_2-Based Resistive Switches at Low Temperature and Voltage

*Jonghan Kwon, Abhishek A. Sharma, James A. Bain, Yoosuf N. Picard, and Marek Skowronski**

Transmission electron microscopy with in situ biasing has been performed on TiN/single-crystal rutile TiO_2/Pt resistive switching structures. Three elementary processes essential for switching: i) creation of oxygen vacancies by electrochemical reactions at low temperatures (<150 °C), ii) their drift in the electric field, and iii) their coalescence into planar faults (and dissociation from them) have been documented. The faults have a form of vacancy discs in {110} and {121} planes, are bound by partial dislocation loops, and are identical to Wadsley defects observed in nonstoichiometric TiO_2 annealed at high temperatures. The faults can be regarded as a precursor to the formation of oxygen-deficient Magnéli phases, but 3D secondary phase inclusions have not been detected. Together, the observations shed light on the behavior of oxygen vacancies in relatively low electric fields and temperatures, suggesting that, in addition to the rather accepted notion of oxygen vacancy motion during the writing processes in resistive switching devices, such motion may occur even during reading, and may be accompanied by significant oxygen vacancy creation at modest device excitation levels.

1. Introduction

Resistive switching (RS) has attracted widespread attention in recent years due to its potential application in next generation nonvolatile memory technology.[1–4] Among several different material systems and mechanisms, bipolar switching in oxide-based devices is of particular interest in this field and the subject of the current study. Oxide-based resistive switching devices consist of metal/oxide/metal sandwiches and exhibit two nonvolatile states of resistance. Switching between these two states can be accomplished by application of electrical biases with opposite polarities.[5] The low resistance ON state is widely attributed to the formation of a conductive path that connects both electrodes. The high resistance state corresponds to a rupture of this path, forming a high resistance gap.[6–9] The conductive path is thought to have the form of a filament with diameters estimated to be between 10 and 100 nm.[10–12] The filaments are not formed during the fabrication of the device. Instead, the as-fabricated structures must go through a one-time conditioning process called electroformation that creates the filament.[5,13] In the case of TiO_2, it is widely believed that the filament consists of one of the oxygen deficient phases known as Magnéli phases with formula Ti_nO_{2-n} ($4 \le n \le 36$), all of which exhibit metallic conductivity.[2,3,14]

The interpretations of the electroformation and resistive switching phenomena summarized above are based on several elementary processes assumed to occur in the metal/insulator/metal (MIM) structures. The first of them is the creation of oxygen vacancies in the functional layer under bias. The process is attributed to electrochemical redox reactions at the oxide/anode interface.[2,13,14] When a doubly positively charged oxygen vacancy is created in TiO_2, two electrons are donated to the conduction band leading to an increase in its conductivity during electroformation.[13] It is important to note that the creation of vacancies in the accepted interpretation precedes current increase, i.e., they are expected to form as the result of the electric field rather than Joule heating due to the current flow. The second elementary process is oxygen vacancy drift in the applied field, leading to the accumulation of vacancies at the cathode. This is followed by the third important process: the reversible coalescence and dissociation of vacancies into and from the secondary phase with well-defined phase boundaries. While there is ample evidence of the drift of oxygen vacancies at low temperatures,[15–17] the evidence for the other two processes is sparse and most of it is indirect.

The issue of vacancy creation in oxides by electrochemical reaction has been thoroughly reviewed by Jeong et al.[2] and Szot et al.[14] One group of experiments, nominally similar to electroformation and switching, induced electrocoloration and electrodegradation in bulk oxides.[15,16,18,19] The electrical bias applied at temperatures between 27 and 230 °C resulted in orders of magnitude decreases in electrical resistance. This resistance drop was attributed to redistribution of pre-existing oxygen vacancies under bias; none of the authors mentioned the creation of vacancies under the applied bias. Observations

J. Kwon, Prof. Y. N. Picard, Prof. M. Skowronski
Materials Science and Engineering Department
Carnegie Mellon University
5000 Forbes Ave., Pittsburgh, PA 15213, USA
E-mail: mareks@cmu.edu
A. A. Sharma, Prof. J. A. Bain
Electrical and Computer Engineering Department
Carnegie Mellon University
5000 Forbes Ave., Pittsburgh, PA 15213, USA

DOI: 10.1002/adfm.201500444

in support of vacancy creation include the formation of bubbles under the anode metal layer.[20,21] The effect was interpreted as due to evolution of oxygen gas from the functional layer. It is clear, however, that this evidence is only indirect and the bubble effect is absent in most nanoscale devices. Lastly, Szot et al.[14] argued that vacancies were formed in bulk TiO_2 samples under low fields (0.01 V cm^{-1}) and high, but unspecified, currents. The current flow in that experiment heated the sample to 500 °C, which is significantly below temperatures where thermally induced reduction is expected to occur.[22] It should be pointed out, however, that the sample was in contact with metallic leads in which case, temperatures as low as 400 °C are adequate for significant oxygen loss in TiO_2.[23] Therefore, observed reduction and electrical resistance changes in oxides could have been of thermal origin.

The third process (reversible coalescence of vacancies into stable agglomerates and their dissolution) is an important feature of the switching process. Since the drift mobility and diffusion coefficient of isolated vacancies are proportional to each other, it is difficult to envision fast switching and long retention. This voltage-time dilemma[24,25] could be reconciled if ion transport becomes nonlinear in high fields (accelerating switching)[26] or if oxygen vacancies form agglomerates (improving retention).[3] One such vacancy agglomerate in TiO_2 are Ti_nO_{2n-1} Magnéli phases reported to be present in some electroformed and switched devices.[10,11,27] However, these observations were made on nonoptimized structures exhibiting high temperature excursions during switching. The crystalline Ti_nO_{2n-1} can be an aftereffect of the high temperatures rather than their cause. In fact, later transmission electron microscopy (TEM) investigations reported absence of Magnéli phases in switched devices.[12] Other than the observations of Magnéli phases at high dissipated power, we have no evidence of the types of agglomerates vacancies could form.

There is, however, ample evidence of vacancies forming agglomerates as a result of high temperature annealing. The periodically arranged 3D vacancy aggregates, i.e., Magnéli phases have been observed in samples prepared by annealing of nonstoichiometric TiO_2 + Ti mixtures at 1150 °C[28] or by melting of TiO_2 powder pellets at 1830 °C.[29,30] Annealing stoichiometric rutile crystals at temperatures up to 1000 °C in vacuum produced only disordered planar faults known as Wadsley defects.[31,32] The reverse process of dissolution of Wadsley defects during annealing in oxidizing ambient has also been reported.[7,33] The study by Kamaladasa et al.[34] have attempted to test whether similar aggregation/dissolution processes can be induced by biasing the metal/single-crystal rutile/metal structure. While they reported formation of Wadsley defects and Magnéli phases, the estimated temperatures in part of the sample exceeded 800 °C posing the question of their origin.

The series of experiments described below have a goal of documenting and quantifying all three elementary processes (vacancy creation, drift, and reversible coalescence/dissolution) involved in resistive switching in rutile by in situ biasing of metal/rutile/metal structures. Use of single-crystal rutile as the functional oxide has made it possible to analyze the induced extended defect creation which would be experimentally difficult in nanocrystalline materials. We report definitive observation of reversible coalescence of oxygen vacancies into extended defects and their dissociation in applied electric field at low temperatures. The correlation of the switching *I–V* characteristics and particular morphology of structural changes is beyond the scope of this study. It is a worthwhile objective and some of this was the subject of our recent publications.[34] However, the switching process in oxides induces large temperature excursions which are further exacerbated by the poor thermal sinking of thin TEM foils. This does not allow for identification of processes which is the objective of this work.

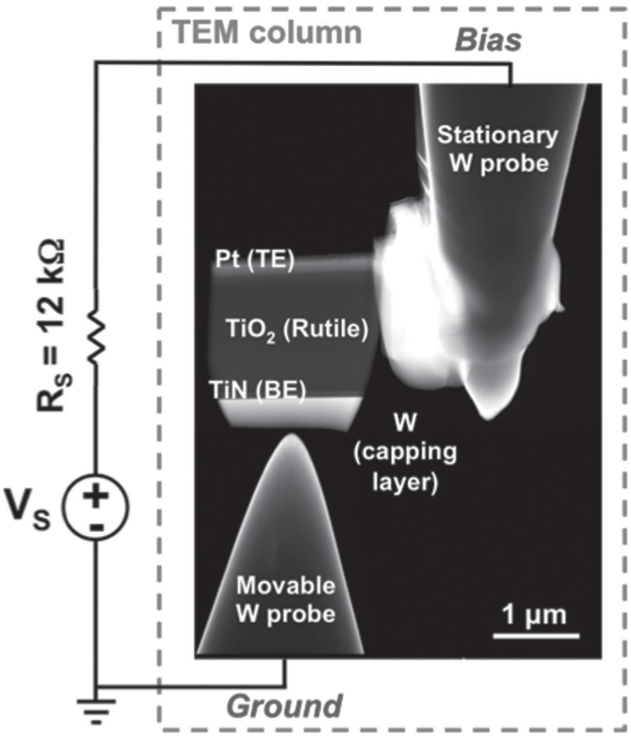

Figure 1. Scanning transmission electron microscopy image (high-angle annular dark field mode) of the Pt/TiO_2/TiN/Mo/W sample mounted on the tungsten probe. The bright contrast between the sample and the probe is due to FIB-deposited Pt weld. Schematic diagram of electrical connections is included.

2. In Situ Biasing TEM Experiments

The complete device structure attached to the tungsten probe is shown in the scanning TEM high angle annular dark-field micrograph in **Figure 1**. Pt and TiN layers are seen as gray contrast, and considering the geometry in the image, these are referred to as top and bottom electrodes, respectively. In all TEM micrographs below, samples are shown in the same orientation as in Figure 1 with bias applied to the top electrode and the bottom electrode (contact made by a movable needle) grounded. This geometry allowed for observations of extended defect dynamics under bias.

3. Microstructure Changes under Bias

Figure 2a shows a bright field TEM micrograph of an as-fabricated Pt/TiO_2/TiN/Mo/W sample before application of a bias.

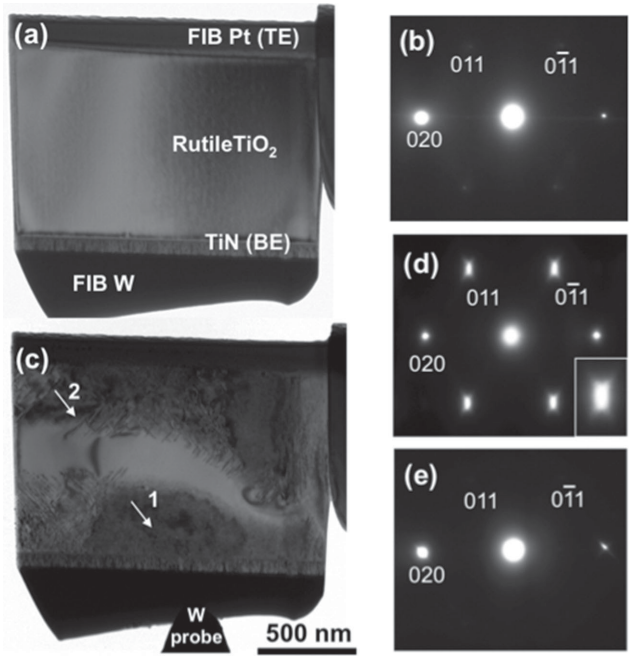

Figure 2. TEM bright field images of a) as-fabricated Pt/TiO_2/TiN device and c) the same device after electrical biasing. b–e) selected area diffraction patterns (SADP) close to two-beam condition for $\boldsymbol{g}$ = 020 near [100] zone axis. Panel (b) corresponds to the as-fabricated structure while (d) and (e) were obtained from location indicated by arrows "1" and "2" in (c). The size of the SADP aperture was 200 nm.

Electron-beam assisted chemical vapor deposited (CVD) Pt electrode and tungsten protective layer are visible as dark areas at the top and bottom of the image. The single-crystal TiO_2 is sandwiched between the Pt and TiN layers. The gradual left to right contrast modulation in rutile is due to sample bending. The dark contrast along the TiO_2/TiN interface is presumably a focused ion beam (FIB)-induced artifact during the Ga^+ ion beam milling. The TiN layer shadows the oxide resulting in a continuous FIB damage layer on the TiO_2 crystal along the interface. It is apparent that our samples prepared this way do not contain any extended defects. This includes any possible secondary inclusions, stacking faults, or dislocations. The absence of dislocations is important as some authors argue for high dislocation density near oxide surfaces,[20] and as these defects have been associated with switching.[5] Figure 2b is a selected area diffraction pattern (SADP) at approximately the two-beam condition for $\boldsymbol{g}$ = 020 near the [100] zone axis, taken at the center of the TiO_2. The pattern corresponds to electron diffraction from the defect-free single-crystal TiO_2 and will serve as a reference to monitor changes induced by application of bias.

Figure 2c is the image of the specimen after a series of quasi-DC sweeps and constant bias stresses with maximum device voltage across the device of ±1.5 V (all voltages are measured across the sample and do not include the drop across the series resistor). This voltage was below the forming voltage and at no point was there a rapid change of resistance, characteristic of the electroformation process. We have deliberately selected the voltage range and the series resistor to prevent the current run away which can result in current filamentation and large local temperature excursion.[35] An example of the resistance change during biasing is shown in Figure S1, Supporting Information. The maximum electric field in the device was 1.5×10^4 V cm^{-1} and the maximum power delivered to the device was less than 0.4 mW. This field is three orders of magnitude lower than one used by Strachan et al. with the similar dissipated power.[12] The resistance of the device decreased from 20 to 7.5 kΩ between Figure 2a and c. This resistance drop is similar to that observed during electrodegradation.[16] The change of contrast in the TiO_2 is apparent: two dark defect zones appeared in proximity of both electrodes with only a narrow strip of material approximately 300–100 nm in width in the center of the TiO_2 remaining free of defects. The nature of the defects was determined from the SADP shown in (d) and (e). The pattern in Figure 2d obtained in the center of the dark contrast area (marked by an arrow "1" in Figure 2c) shows multiple {011} streaks. The streaking suggests presence of planar faults in the sample along (011) and $(0\bar{1}1)$ planes. The streaking depends on the location in the sample. For example, the SADP collected at the edge of the defect zone (marked by arrow "2" in Figure 2c) exhibits one dominant streak along the (011) direction indicating the presence of only one set of planar faults parallel to (011). The intensity of the streak is weaker than in Figure 2d consistent with the expected lower density of faults at the edge of the defect region. The appearance of streaks rather than discrete superlattice reflections[30] indicates a random rather than a periodic distribution of faults. Planar faults in {110} planes of rutile are well known and have been analyzed in detail by TEM.[29] These defects correspond to missing {110} planes of oxygen atoms and are referred to as Wadsley defects.[30] The faults appear in rutile crystals reduced at temperatures above 1000 °C and are known to be created by coalescence of oxygen vacancies. The vacancies can also coalesce on {121} and {132} planes creating different families of Wadsley defects.[30]

The defect zones in Figure 2c extend along both electrodes roughly reflecting the expected distribution of electrostatic potential in the biased sample. The slight asymmetry could be due to differences in local temperature caused by tungsten probes acting as heat sinks and/or changes on sample thickness locally affecting resistance. In most locations within the defect zones in heavily stressed (electrically) samples, the defect densities were too high to resolve individual faults. The low fault density area at the edge of the defect zone in Figure 2c is analyzed in more detail in Figure 4.

The identification of contrast as due to missing planes of oxygen atoms is further supported by micrographs shown in **Figure 3**. Figure 3a is a bright field TEM micrograph of another specimen after a series of gradually increasing quasi-DC sweep magnitude from 0 to −1.1 V (note: only negative bias was applied to the top electrode). The bias resulted in formation of only one defect zone in proximity of the top electrode (the diffuse dark bands in the middle and the right bottom of the TiO_2 are bend contours). In all experiments, the defects always appeared at the negatively biased electrode whether it was Pt or TiN. This behavior is consistent with faults formed by coalescence of positively charged point defects such as oxygen vacancies drifting in the applied electric field and accumulating close to the cathode as first suggested by Kim et al.[36] and later widely accepted.[13] The biasing was stopped at initial stages (lower field

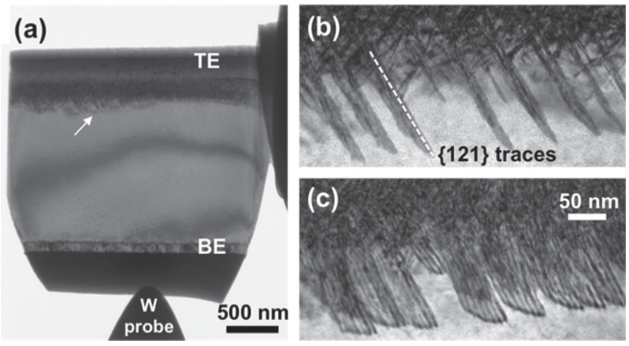

Figure 3. a) BF TEM image of electrically stressed specimen at the early stages of degradation. b) A magnified view of the region pointed out by an arrow in (a). c) The same location as (b) with the specimen tilt exposing the defect planes.

and shorter time than in Figure 2) and the individual defects can be resolved at the edge of the defect region. They appear as narrow lines along (121) traces on the surface of (100) oriented sample, i.e., the image represents the planar (121) Wadsley defects viewed edge on. The morphology of the faults can be seen in Figure 3c obtained by tilting the specimen by about 15° around a vertical axis (α-tilt). What was the set of straight-lines, now appears as a series of 2D defects with characteristic striped contrast of a planar fault.[37] All of the characteristics of defects observed in our samples appear to be consistent with those of Wadsley defects reported in reduced TiO_2.[30]

Wadsley defects observed in our experiments if arranged in a periodic fashion can form one of the Magnéli phases.[29,38] One can think of them as the initial step toward creation of such phases and in this sense our results are in agreement with those of Kwon et al.[10] Nevertheless, one needs to address the question why Magnéli phases were not observed even after prolonged biasing of the samples. The likely reason lies in the much lower dissipated power density in our structures. In experiment by Kwon et al.,[10] the current flow was restricted to the narrow filament with the maximum dissipated power during the RESET process of over 20 mW. The corresponding local Joule heating caused the temperature increase to be high enough to change the morphology of the top electrode and possibly melt it. The estimated temperature of the 200 nm diameter TiO_{2-x} filament with such power dissipation exceeds 3700 °C.[39] Formation of Magnéli phases in such conditions ($T > 1500$ °C) would be consistent with experiments of Bursill et al.[29] It should be noted that our earlier publication reported formation of Magnéli phases in conditions of switching runaway.[34]

It is apparent that there are no Wadsley defects or any other oxygen vacancy agglomerates in the rutile crystal of the as-fabricated structure shown in Figure 2a. It implies that the concentration of oxygen vacancies is below the solid solubility limit which was estimated at $x = 0.0015$ in TiO_{2-x},[32] and which corresponds to the vacancy concentration of 4.8×10^{19} cm^{-3}. The vacancy density estimated from measured electrical conductivity (assuming electron mobility value of 1 μm V s^{-1})[40] was 7.8×10^{18} cm^{-3}. It is also apparent that the vacancy concentration in the sample after electrical biasing exceeded the solubility limit causing the vacancies to precipitate out and form Wadsley defects. Since the defected areas in the sample constitute over 80% of the total sample volume, one can argue that the total vacancy concentration exceeded total solubility. We can therefore conclude that oxygen vacancies were created under our experimental conditions. As the biasing progressed, the total number of vacancies in the sample gradually increased. This could be expected, as in the ultra-high vacuum environment the oxygen atom once lost cannot be replaced. On the other hand though, locally we have observed repeated processes of oxidation and reduction as the bias was reversed (**Figure 4**, below). The last step necessary to prove the vacancy creation by electrochemical reaction (not thermal origin) is the temperature estimate. This is discussed in detail in Section 5 with the conclusion that the temperature during our experiments does not exceed 150 °C. This is significantly below the temperature necessary to reduce TiO_2 in contact with a getter layer (≈400 °C), providing the most compelling evidence so far for electrochemical reaction-induced creation of vacancies in resistive switching devices.

4. Coalescence and Desorption of Vacancies from Planar Faults

The typical testing method of switching devices employs quasi-DC sweeps with the predetermined voltage range. At some point during the sweep, the resistance of the device rapidly changes during the SET and RESET events. Concomitantly, the filament is expected to change its length or cross section. This type of behavior was reported by Kamaladasa et al.: the rapid change of resistance was associated with major changes of the sample microstructure.[34] While informative in their own right,

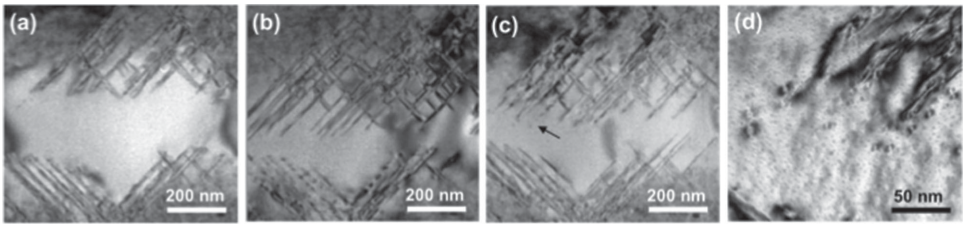

Figure 4. High magnification images of the region marked by arrow "2" in Figure 2c during in situ constant bias stress. a,b) max. V = –1.35 V applied between (a) and (b) for 300 s. b,c) max. V = +1.15 V applied between (b) and (c) for 300 s. (a,b) Growth of the top defect zone and dissociation of the bottom defect zone. (b,c) Dissociation of the top defect zone and growth of the bottom defect zone. d) Magnified views of arrowed region in (c) showing dislocation loops (coffee bean-like contrast) near the end of the Wadsley defects. The small gray speckles shown in (d) are to be believed Ga droplets with Ga deposited during the FIB sample preparation and aggregated during the experiment.[44] Note that the specimen was tilted when imaging (d).

such events are difficult to analyze from the perspective of the mechanisms involved since the electroformation and switching events typically are associated with large local temperature excursions.[12,35,39] We elected to bias the devices at constant source voltage in order to eliminate such excursions and focus on effects of the electric field (the evolution of sample resistance under bias is shown in Figure S1, Supporting Information). The evolution of Wadsley defects under constant source voltage was recorded in two-beam condition for $\boldsymbol{g}$ = 020. Figure 4 is the high magnification image of the region marked with arrow "2" in Figure 2c. The images (a)–(c) show the same area of the sample with the two regions of Wadsley defects facing each other. The micrograph in (a) corresponds to the starting point with (b) taken after 300 s of –1.35 V applied to the top electrode. (Note that the voltage across the device decreased to –0.85 V during the experiment due to a change in the device resistance (see the Supporting Information). Comparing the two images, it is apparent that Wadsley defects (dark straight lines) at the top defect zone extended downward, narrowing the gap. The faults increased in length by an average of 135 nm. Since the faults are nonconservative (they change local composition of the material) with the displacement vector out of the plane of the fault,[38,41] such extension must be associated with the absorption of oxygen vacancies. The process occurs one vacancy at the time attaching to the edge of the missing plane of oxygen ions with crystallography of the process described by Anderson and Hyde[41] and Bursill and Hyde.[30] The defect zone in the lower part of the specimen serves here as the reservoir of vacancies.

In the same pair of micrographs, the faults at the edge of the bottom defect zone retracted somewhat and faults changed contrast from continuous lines to "dashed" ones. The behavior of the faults in the lower defect zone is not obvious. One could expect the vacancies to desorb from the edges of Wadsley defects. Such process, if repeated, would result in a gradual contraction of the fault and would be the exact opposite to the fault extension occurring in the upper defect zone. Rather than this, the contrast change indicates the planar faults breaking up into numerous small defects with sizes of about 10 nm lying in the same plane and giving a "dashed" line appearance. While this behavior effectively lowers the fault area and the total number of vacancies aggregated into faults, it increases the length of partial dislocations bounding the faults. Observation of similar contrast associated with thermal dissolution of Wadsley defects has been reported by Blanchin and Bursill.[7,42] Specifically, these authors reported Wadsley defects dissociating into dash-like "small defects." The structure of these is likely that of a disc of vacancies bound by the dislocation loop. This assertion is supported by the image in Figure 4d obtained by tilting the sample by about 15° about the vertical axis (α-tilt). The small defects produce a characteristic "coffee bean"-like contrast that is known to correspond to strain contrast of a small dislocation loop.[43] It was impossible to determine the Burgers vector and the plane normal of the loops due to the limited tilt of the single-tilt axis TEM holder. The incomplete retraction of defects under bias can have important consequences for the endurance or reliability of switching devices. Leaving "debris" behind the retracing faults would lead to slow accumulation of vacancies, gradually affect the device characteristics and even result in eventual RESET failures. It should be noted here that the extension and retraction of faults has been observed repeatedly upon reversal of the bias polarity. This corresponds to repeated local oxidation and reduction of the sample.

The image shown in Figure 4c was obtained after application of positive 1.15 V bias for 300 s (compared to Figure 4b). Similar to the negative biasing, we observed a voltage drop to 0.76 V during the experiment. The changes of the microstructure are basically the reversal of the changes between images (a) and (b). Since the temperature during the experiments did not exceed 150 °C (see Section 5), this proves that vacancies can detach themselves from the Wadsley defects under the influence of the electric field. Also, it is quite obvious from Figure 4a–c that the vacancies drift in the electric field and coalesce to form faults. This proves the second and the third elementary processes responsible for resistive switching do occur.

5. Temperature Estimates

Most of the processes discussed above are likely to be thermally activated. The device temperature is of importance for the current study as we would like to decouple defect dynamics due to temperature and voltage. In order to estimate the temperature changes due to Joule heating, a 3D heat flow simulation was performed using COMSOL Multiphysics package. Built-in "electric current" and "heat transfer in solids" modules were coupled for the steady-state simulations. These modules solve the heat diffusion equation and Maxwell's equations simultaneously to yield a self-consistent temperature estimate. **Figure 5** shows the thermal profile of the simulated device. The peak temperature reached is 143 °C and this is the highest temperature during the entire biasing experiments. The temperature

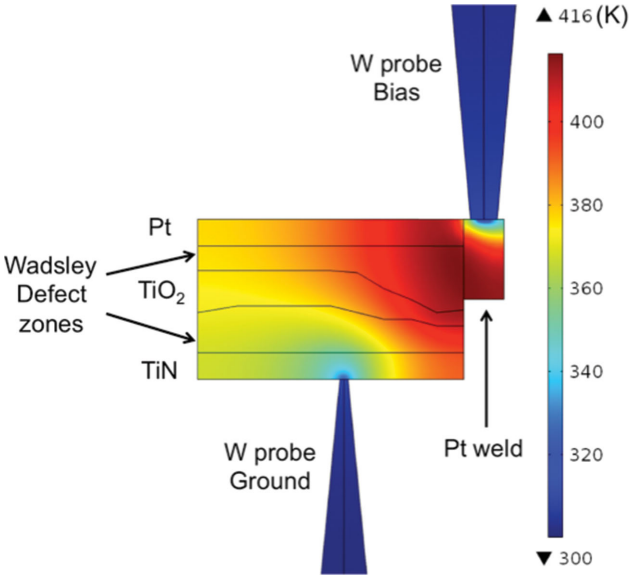

Figure 5. The temperature profile of the specimen during the in situ biasing experiment performed via COMSOL Multiphysics. The peak temperature is 143 °C (416 K). Note that the temperature near the location where the concurrent growth and dissociation of Wadsley defect occurs is lower (107 °C (380 K)) than the peak temperature.

near the location where the concurrent growth and dissociation of Wadsley defect occurs is 107 °C.

6. Discussion

It is quite clear from Figures 2–4 that the vacancies/Wadsley defects never form a small diameter filament. The defect zone boundaries in our samples are roughly parallel to the two electrodes and do not approach each other by less than 50 nm. This is in stark contrast with the expectation that the filament is more or less cylindrical with the diameter in the 1–10 nm range.[9,10] The possible origins of the different "filament" shape could be a difference in field strength, and a different sample geometry compared to standard switching devices: the large thickness of the oxide, relatively flat interfaces between electrodes and the oxide, and very different heat sinking. Another significant difference is the proximity of the sample surfaces making it easy for the oxygen ions to leave the functional layer. We do not think, however, that this is a dominant effect as the TEM micrographs show the defect distribution being uniform throughout the sample thickness. The nonuniformities are rather associated with the electrodes as seen in the micrographs. Many of these differences are unavoidable consequences of the in situ experiment. Also different were electroforming/switching procedures used in our experiments. Typically, electroforming and switching are induced using a quasi-DC voltage sweep. At some point during the sweep, the resistance changes rapidly due to electronic instabilities of the structures. As shown by Sharma et al.,[35] the TaO_x-and TiO_x-based devices exhibit negative differential resistance in part of their *I–V* characteristics. This leads to a rapid spontaneous constriction of current flow, local Joule heating, and formation of a small diameter filament. The MIM structures used in this experiment do not show such *I–V* characteristics.

The values of the voltage used in our experiments causing the vacancy formation and redistribution are surprisingly small (1–2 V). They are, however, in the same range as electroformation and switching voltages reported in number of devices based on TiO_2,[21,39] Ta_2O_5,[45] or HfO_2.[46] It is also widely accepted that the operating mechanism is the electrochemical reaction. The energetics of such reactions remain to be worked out and will likely require a much better understanding of the electrostatic potential distribution in switching structures.

Lastly, the question arises whether the process reported here could be active in typical switching devices comprising amorphous or nanocrystalline functional layers. We would like to argue this is the case. While the amorphous oxide films lack of long range order, they have a similar short range one. It is easy to imagine formation of oxygen vacancy clusters in amorphous materials that correspond to Wadsley defects in single-crystals of rutile. Locally, the Wadsley defect corresponds to transition between edge-sharing octahedra in the stoichiometric crystal to face-sharing ones.[47] This preserves the coordination of all atoms affecting only farther neighbors; such change can easily occur in amorphous or nanocrystalline materials. Of course, the coalescence in a single-crystal occurs on a well-defined crystal plane and the resulting defects have a large spatial extent. In amorphous or nanocrystalline material, the planes will not be well defined and the size of vacancy clusters is likely limited reminiscent possibly of "small oxygen vacancy defects" reported by Blanchin and Bursill.[7,42] It is quite apparent that the local structure of such defects can be almost identical in single-crystals and amorphous films. In both materials, the net electrical effect of the oxygen deficiency is very similar: titanium will retain more of its electrons populating the states in the conduction band and increasing the conductivity.

The lateral size of the Wadsley defects seen in Figure 3 is over 100 nm. Clearly there are no well-defined planes of this size in amorphous materials. As a consequence, the vacancy agglomerates would have to be smaller. It is well documented that vacancy agglomerates even in single-crystals come in a continuous distribution of sizes with clusters as small as just several anion vacancies reported.[7,42,48] It appears then quite possible to form similar clusters in either amorphous or nanocrystalline thin films.

Another important aspect of our observations is the relatively low value of electric field causing creation, drift, and coalescence of vacancies ($\approx 1 \times 10^4$ V cm^{-1}). A 10 mV *Read* pulse applied to a 10 nm thick oxide layer would induce fields well in excess of the fields used in our experiments. Therefore, the defect dynamics reported here can be important under *Read* and *Disturb* voltages for nanoscale RS devices.

7. Conclusions

We have investigated electric field-induced defect reactions in a prototypical resistive switching system consisting of single-crystal rutile TiO_2 sandwiched between Pt and TiN electrodes. Careful biasing limited the Joule heating of the specimens to no more than 150 °C. Three elementary processes (creation, drift, and reversible coalescence/dissociation of vacancies) essential for the functioning of resistive switching devices have been documented by direct in situ biasing TEM observations.

Oxygen vacancy creation at the applied electric field of 1.5×10^4 V cm^{-1} was documented as the increase of the vacancy content above the solid solubility limit of $x = 0.0015$ in TiO_{2-x} throughout most of the TiO_2 volume. The vacancies coalesced into planar defects on {110} and {121} planes referred to as Wadsley defects. Repeated bias sweeps of both polarities created two defect zones adjacent to both electrodes. Upon changing the bias polarity, the extended faults near the anode dissociated and contracted by emission of oxygen vacancies. The point defects drifted in the applied field, attached themselves to the edges of faults in the defect zone near the cathode, and agglomerated so that fault lengths were extended.

Thus, we have extended a methodology demonstrated by Yang et al.[49] in the case of conducting bridge mechanism to a devices exhibiting valence change mechanism. The dynamic defect analysis in this model system can contribute to further understanding in resistive switching mechanism of TiO_2-based resistive random-access memory (RRAM) and also in other nonstoichiometric transition metal oxide systems. Specifically, this sheds light on the possibility of creation of oxygen vacancies at low-biases and temperatures which are conditions akin to *Read* and *Disturb*. Moreover, incomplete retraction of defects

in presence of field also indicates this as being a possible mechanism for RESET failures after endurance cycling.

8. Experimental Section

The functional oxide for the investigated structures was single-crystalline rutile (MTI Corporation (Richmond, CA)). 100 nm thick Ti getter film was sputter deposited on the backside of the crystal followed by annealing at 500 °C at 1×10^{-8} Torr for 1 h. The annealing reduced the crystal with the conductivity increasing from 50 S m^{-1} to 250 S m^{-1}. This gives the density of doubly ionized oxygen vacancies of 7.8×10^{18} cm^{-3} (assuming electron mobility of 1 cm^2 V s^{-1}).[40] A stack of 80 nm TiN film followed by 20 nm of molybdenum was sputtered as a bottom electrode (samples were inverted for TEM experiments). TEM specimens (about $2 \times 1 \times 1.5$ µm in size) were lifted-out in FEI Nova 600 Nanolab focused ion beam (FIB) and affixed to tungsten needles. The top electrode was an electron beam-assisted chemical vapor deposition (CVD) platinum deposited by FIB. The slabs were then thinned down to electron transparency (≈150 nm) with 30 keV Ga+ beam and finished with 5 keV polishing step (≈100 nm). It is known that the 5 keV ion polishing step during sample preparation leaves a thin amorphous layer on the sample surfaces. The thickness of such a layer in single-crystal Si prepared in similar manner was estimated at 10 nm.[50] While this amorphous overlayer has somewhat degraded the image quality, it still allowed for observation of structural changes in the device.

The in situ biasing TEM experiments were performed in the FEI Tecnai F20 microscope operated at 200 keV with a Nanofactory in situ biasing holder (single-tilt). Two-beam bright-field (BF) imaging was utilized to observe formation and evolution of extended defects. A schematic with the scanning TEM (STEM) high-angle annular dark field (HAADF) image in Figure 1 illustrates the in situ biasing TEM setup used in this study. Two tungsten scanning tunneling microscope (STM) probes were mounted in the TEM holder facing each other. The stationary STM probe where the specimen was attached was electrically biased. The piezo-driven nanomanipulated STM probe was grounded in all experiments.

An Agilent Semiconductor Parameter Analyzer 4156C was utilized to apply quasi-DC sweeps and constant bias across the $Pt/TiO_2/TiN$ stack. The constant bias in this study refers to the source voltage and the voltage across the device (always lower than the source voltage due to a series resistor) represents the voltage appearing across the device. We monitor a decrease in device voltage as the resistance of the device decreases over time (see Figure S1, Supporting Information). An external series resistor of 12 kΩ was connected to the circuit to suppress current run away leading to rapid resistance changes in the device and thus prevented large local temperature excursions.

Acknowledgements

The authors thank Tom Nuhfer and Prof. Marc De Graef for assistance with TEM analysis. This work was supported by NSF Grant No. DMR1409068 and SRC Contract No. 2012-VJ-2247.

Received: February 2, 2015
Revised: March 7, 2015
Published online: March 30, 2015

[1] H.-S. P. Wong, H.-Y. Lee, S. Yu, Y.-S. Chen, Y. Wu, P.-S. Chen, B. Lee, F. T. Chen, M.-J. Tsai, *Proc. IEEE* **2012**, *100*, 1951.
[2] D. S. Jeong, R. Thomas, R. S. Katiyar, J. F. Scott, H. Kohlstedt, A. Petraru, C. S. Hwang, *Rep. Prog. Phys.* **2012**, *75*, 076502.
[3] J. J. Yang, D. B. Strukov, D. R. Stewart, *Nat. Nanotechnol.* **2013**, *8*, 13.
[4] B. J. Choi, D. S. Jeong, S. K. Kim, C. Rohde, S. Choi, J. H. Oh, H. J. Kim, C. S. Hwang, K. Szot, R. Waser, B. Reichenberg, S. Tiedke, *J. Appl. Phys.* **2005**, *98*, 033715.
[5] R. Waser, R. Dittmann, G. Staikov, K. Szot, *Adv. Mater.* **2009**, *21*, 2632.
[6] J. Borghetti, D. B. Strukov, M. D. Pickett, J. J. Yang, D. R. Stewart, R. S. Williams, *J. Appl. Phys.* **2009**, *106*, 124504.
[7] M. G. Blanchin, L. A. Bursill, *Phys. Status Solidi* **1984**, *86*, 491.
[8] K. M. Kim, B. J. Choi, M. H. Lee, G. H. Kim, S. J. Song, J. Y. Seok, J. H. Yoon, S. Han, C. S. Hwang, *Nanotechnology* **2011**, *22*, 254010.
[9] S. Larentis, S. Member, F. Nardi, S. Balatti, D. C. Gilmer, D. Ielmini, S. Member, A. Resistive-switching, *IEEE Trans. Electron Devices* **2012**, *59*, 2468.
[10] D.-H. Kwon, K. M. Kim, J. H. Jang, J. M. Jeon, M. H. Lee, G. H. Kim, X.-S. Li, G.-S. Park, B. Lee, S. Han, M. Kim, C. S. Hwang, *Nat. Nanotechnol.* **2010**, *5*, 148.
[11] J. P. Strachan, M. D. Pickett, J. J. Yang, S. Aloni, A. L. David Kilcoyne, G. Medeiros-Ribeiro, R. Stanley Williams, *Adv. Mater.* **2010**, *22*, 3573.
[12] J. P. Strachan, D. B. Strukov, J. Borghetti, J. J. Yang, G. Medeiros-Ribeiro, R. S. Williams, *Nanotechnology* **2011**, *22*, 254015.
[13] D. S. Jeong, H. Schroeder, U. Breuer, R. Waser, *J. Appl. Phys.* **2008**, *104*, 123716.
[14] K. Szot, M. Rogala, W. Speier, Z. Klusek, A. Besmehn, R. Waser, *Nanotechnology* **2011**, *22*, 254001.
[15] R. Waser, T. Baiatu, K.-H. Hardtl, *J. Am. Ceram. Soc.* **1990**, *73*, 1654.
[16] S. Rodewald, J. Fleig, J. Maier, *J. Am. Ceram. Soc.* **2000**, *83*, 1969.
[17] W. Jiang, M. Noman, Y. M. Lu, J. A. Bain, P. A. Salvador, M. Skowronski, *J. Appl. Phys.* **2011**, *110*, 034509.
[18] J. Blanc, D. L. Staebler, *Phys. Rev. B* **1971**, *4*, 3548.
[19] M. Wojtyniak, K. Szot, R. Wrzalik, C. Rodenbücher, G. Roth, R. Waser, *J. Appl. Phys.* **2013**, *113*, 083713.
[20] K. Szot, W. Speier, G. Bihlmayer, R. Waser, *Nat. Mater.* **2006**, *5*, 312.
[21] J. Joshua Yang, F. Miao, M. D. Pickett, D. a a Ohlberg, D. R. Stewart, C. N. Lau, R. S. Williams, *Nanotechnology* **2009**, *20*, 215201.
[22] W. D. Ohlsen, O. W. Johnson, *J. Appl. Phys.* **1973**, *44*, 1973.
[23] J. J. Yang, J. P. Strachan, Q. Xia, D. A. A. Ohlberg, P. J. Kuekes, R. D. Kelley, W. F. Stickle, D. R. Stewart, G. Medeiros-Ribeiro, R. S. Williams, *Adv. Mater.* **2010**, *22*, 4034.
[24] H. Schroeder, V. V. Zhirnov, R. K. Cavin, R. Waser, *J. Appl. Phys.* **2010**, *107*, 054517.
[25] M. Noman, W. Jiang, P. A. Salvador, M. Skowronski, J. A. Bain, *Appl. Phys. A* **2011**, *102*, 877.
[26] D. B. Strukov, R. S. Williams, *Appl. Phys. A Mater. Sci. Process.* **2009**, *94*, 515.
[27] K. M. Kim, S. J. Song, G. H. Kim, J. Y. Seok, M. H. Lee, J. H. Yoon, J. Park, C. S. Hwang, *Adv. Funct. Mater.* **2011**, *21*, 1587.
[28] S. Andersson, B. Collén, G. Kruuse, U. Kuylenstierna, A. Magnéli, H. Pestmalis, S. Åsbrink, *Acta Chem. Scand.* **1957**, *11*, 1653.
[29] L. A. Bursill, B. G. Hyde, O. Terasaki, D. Watanabe, *Philos. Mag.* **1969**, *20*, 347.
[30] L. A. Bursill, B. G. Hyde, *Prog. Solid State Chem.* **1972**, *7*, 177.
[31] L. A. Bursill, B. G. Hyde, *Philos. Mag.* **1971**, *23*, 3.
[32] M. G. Blanchin, P. Faisant, C. Picard, M. Ezzo, G. Fontaine, *Phys. Status Solidi* **1980**, *60*, 357.
[33] L. A. Bursill, S. G. Jun, D. J. Smith, M. G. Blanchin, *Ultramicroscopy* **1984**, *13*, 191.
[34] R. J. Kamaladasa, A. A. Sharma, Y.-T. Lai, W. Chen, P. A. Salvador, J. A. Bain, M. Skowronski, Y. N. Picard, *Microsc. Microanal.* **2015**, *21*, 140.
[35] A. A. Sharma, M. Noman, M. Abdelmoula, M. Skowronski, J. A. Bain, *Adv. Funct. Mater.* **2014**, *24*, 5522.

[36] K. M. Kim, B. J. Choi, Y. C. Shin, S. Choi, C. S. Hwang, *Appl. Phys. Lett.* **2007**, *91*, 012907.
[37] D. B. Williams, C. B. Carter, *Transmission Electron Microscopy*, 2nd ed., Springer, New York **2009**, p. 760.
[38] L. A. Bursill, B. G. Hyde, D. K. Philp, *Philos. Mag.* **1971**, *23*, 1501.
[39] Y. Meng Lu, M. Noman, Y. N. Picard, J. A. Bain, P. A. Salvador, M. Skowronski, *J. Appl. Phys.* **2013**, *113*, 163703.
[40] E. Yagi, R. R. Hasiguti, M. Aono, *Phys. Rev. B* **1996**, *54*, 7945.
[41] J. S. Anderson, B. G. Hyde, *J. Phys. Chem. Solids* **1967**, *28*, 1393.
[42] M. G. Blanchin, L. A. Bursill, *Phys. Status Solidi* **1984**, *86*, 101.
[43] T. Suzuki, M. Ueno, Y. Nishi, M. Fujimoto, *J. Am. Ceram. Soc.* **2001**, *84*, 200.
[44] P. Philipp, L. Bischoff, B. Schmidt, *Nanotechnology* **2012**, *23*, 475304.
[45] S. Kim, S. Choi, W. Lu, *ACS Nano* **2014**, *8*, 2369.
[46] F. Nardi, S. Member, S. Larentis, S. Balatti, D. C. Gilmer, D. Ielmini, S. Member, *IEEE Trans. Electron Devices* **2012**, *59*, 2461.
[47] S. Andersson, A. D. Wadsley, *Nature* **1966**, 581.
[48] M. G. Blanchin, L. A. Bursill, D. J. Smith, *Proc. R. Soc. London, Ser. A* **1984**, *391*, 351.
[49] Y. Yang, P. Gao, L. Li, X. Pan, S. Tappertzhofen, S. Choi, R. Waser, I. Valov, W. D. Lu, *Nat. Commun.* **2014**, *5*, 4232.
[50] L. Pastewka, R. Salzer, A. Graff, F. Altmann, M. Moseler, *Nucl. Instrum. Methods Phys. Res., Sect. B* **2009**, *267*, 3072.